

Neural Network Learning Predicts Optic Flow Specificities of Zebrafish Pretectal Neurons

Gerrit A. Ecke, Fabian A. Mikulasch,
Sebastian A. Bruijns, Thede Witschel,
Aristides B. Arrenberg, and Hanspeter A. Mallot

Dept. of Biology, University of Tübingen, Tübingen, Germany
hanspeter.mallot@uni-tuebingen.de

Abstract. Zebrafish pretectal neurons exhibit specificities for large-field optic flow patterns associated with rotatory or translatory body motion. We investigate the hypothesis that these specificities reflect the input statistics of natural optic flow. Realistic motion sequences are generated with computer graphics simulating self-motion in an underwater scene. Local retinal motion was estimated with a motion detector and encoded in four populations of directionally tuned retinal ganglion cells, represented as two signed input variables. This activity was then used as input into one of two learning networks: a sparse coding network (competitive learning) and backpropagation network (supervised learning). Both simulations develop specificities for optic flow which are comparable to those found in a neurophysiological study [7], and relative frequencies of the various neuronal responses are best modelled by the sparse coding approach. We conclude that the optic flow neurons in the zebrafish pretectum do reflect the optic flow statistics. The predicted vectorial receptive fields show typical optic flow fields but also “Gabor” and dipole-shaped patterns that likely reflect difference fields needed for reconstruction by linear superposition.

1 Introduction

Optimality of visual receptive fields. In his “*neuron-doctrine for perceptual psychology*”, Horace Barlow [3] suggests that the “*nervous system is organized to achieve as complete a representation of the sensory stimulus as possible with the minimum number of active neurons*”. This idea also underlies a number of theoretical approaches to visual processing, such as information maximization, sparse coding, predictive coding, etc.; for a recent overview see [4]. While the general approach is widely accepted, specific predictions about the optimal processing scheme will depend on the choice of the optimality criterion employed as well as on the information requirements of each species’ life-style. Empirical tests of optimal coding theories of visual processing are therefore often limited to a qualitative level. For the case of mammalian V1 cortex, Olshausen

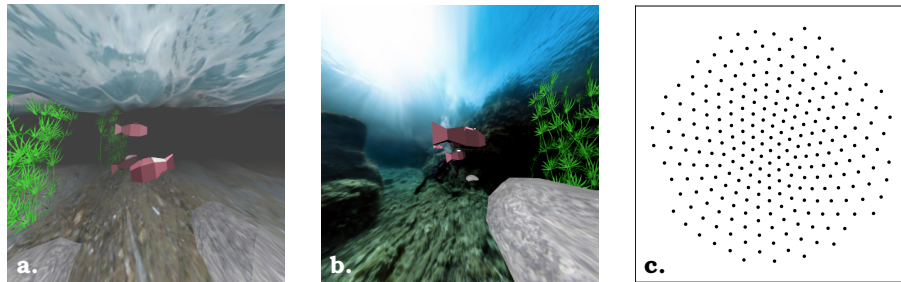


Fig. 1. **a.** View of the virtual fish tank with muddy water (low viewing distance). Additional fish and plants will generate optic flow discontinuities. **b.** Example with high visibility. **c.** Mosaic of retinal ganglion cells, used to calculate the motion input.

and Field [11] have summarized the evidence and concluded that for a full understanding of the system, simultaneous measurements of the activities of a large, unbiased set of neurons in response to natural stimuli would be required.

We attempt an analysis of this type for the area pretectalis (APT) of the zebrafish, where the response of thousands of neurons has indeed been recorded while the fish is presented with optic flow stimuli [7]. Experimentally found response properties from a large, representative sample of neurons will be compared to responses predicted from receptive fields of nodes in an artificial neural network trained with optic flow patterns that were generated by simulating observer movement in a virtual fish tank. The receptive field predictions will be based on two theoretical approaches, (i) sparse coding of optic flow patterns and (ii) supervised learning of ego-motion parameters from the same optic flow patterns.

Optic flow. Like many other animals, zebrafish larvae generate optokinetic responses of the eyes (OKR) and optomotor responses of the body (OMR) when exposed to visual stimuli simulating egomotion of the fish [7,2]. Both eye- and body movements generate on the retina space-variant patterns of local motion vectors that have to be analyzed by subsequent processing stages. Neural algorithms suggested for optic flow analysis usually consist of at least two components, a local motion detector and a subsequent set of templates or motion models for identifying typical patterns relating to ego-motion maneuvers or encounters with obstacles and self-moving objects such as prey or predator [13,6]. Local motion detection can take place in the retina itself, as is generally the case in lower vertebrates, or in early areas of visual cortex. Higher brain areas analyzing optic flow patterns such as the focus of expansion, rotational vertices, left or right yaw rotations, etc., have been identified in mammalian MST cortex [12] or in the zebrafish area pretectalis, APT [7]. In

our model, local visual motion is encoded in the direction-specific tuning curves of retinal ganglion cells and is not subject to learning. Output from the retinal ganglion cells is then fed into a layer of simulated APT-neurons which develop optic flow analyzers.

Zebrafish visual system. Zebrafish retinal ganglion cells (RGCs), as well as pretectal cells, exhibit clear tuning to the direction and orientation of drifting gratings [1]. Movement direction is not covered homogeneously, but clustered around three or four major visual field directions [8]. The larval zebrafish retina contains some 4000 ganglion cells with an average angular separation of about 2.5 degrees of visual angle.

RGCs project to APT, among other targets. The response characteristics of APT neurons have been analyzed with visual stripe pattern (drifting gratings) moving either forward or backward and presented to the left, right, or both eyes [7]. Activity of *monocular* neurons depends only on the stimulus delivered to one eye and can therefore be considered to be directly driven from this eye's RGCs. In contrast, *binocular neurons* combine input from both eyes to generate specificities to forward or backward translation as well as to clockwise and counter-clockwise rotation in the horizontal plane.

2 Visual Front End

Realistic optic flow stimuli are generated from a virtual reality simulation of observer motion in a fish tank, programmed in *blender*¹. The head of the fish was modeled by two cameras rigidly moving together with a rotation center somewhat behind the eyes. The field of view was 160 by 160 degrees with a binocular overlap of 45 degree (see [7]). This results in central viewing directions of ± 57.5 degree for the left and right eye.

The virtual fish-tank contains objects at various distances from the observer as well as objects in mid-water (floating plants and passing fish) generating optic flow discontinuities in translational egomotion (Figure 1a,b). Note that translatory optic flow depends on object distance whereas rotatory optic flow does not. Visibility was set either low (muddy water, Fig. 1a) or high (clear water, Fig. 1b). Overall, the scenery was built to resemble the natural habitat of zebrafish as described in [16].

Virtual fish were placed randomly in the environment and accelerated by a short, random impulse both for translation and rotation. Acceleration for all six degrees of freedom (DoF) were drawn independently from a uniform, zero mean distribution, with an additional scaling factor for the rotatory DoFs introduced in order to equalize the average flow vector lengths of rotatory and translatory flow components. After the acceleration impulse, the motion declined exponentially and a two-frame motion

¹ <https://www.blender.org/>

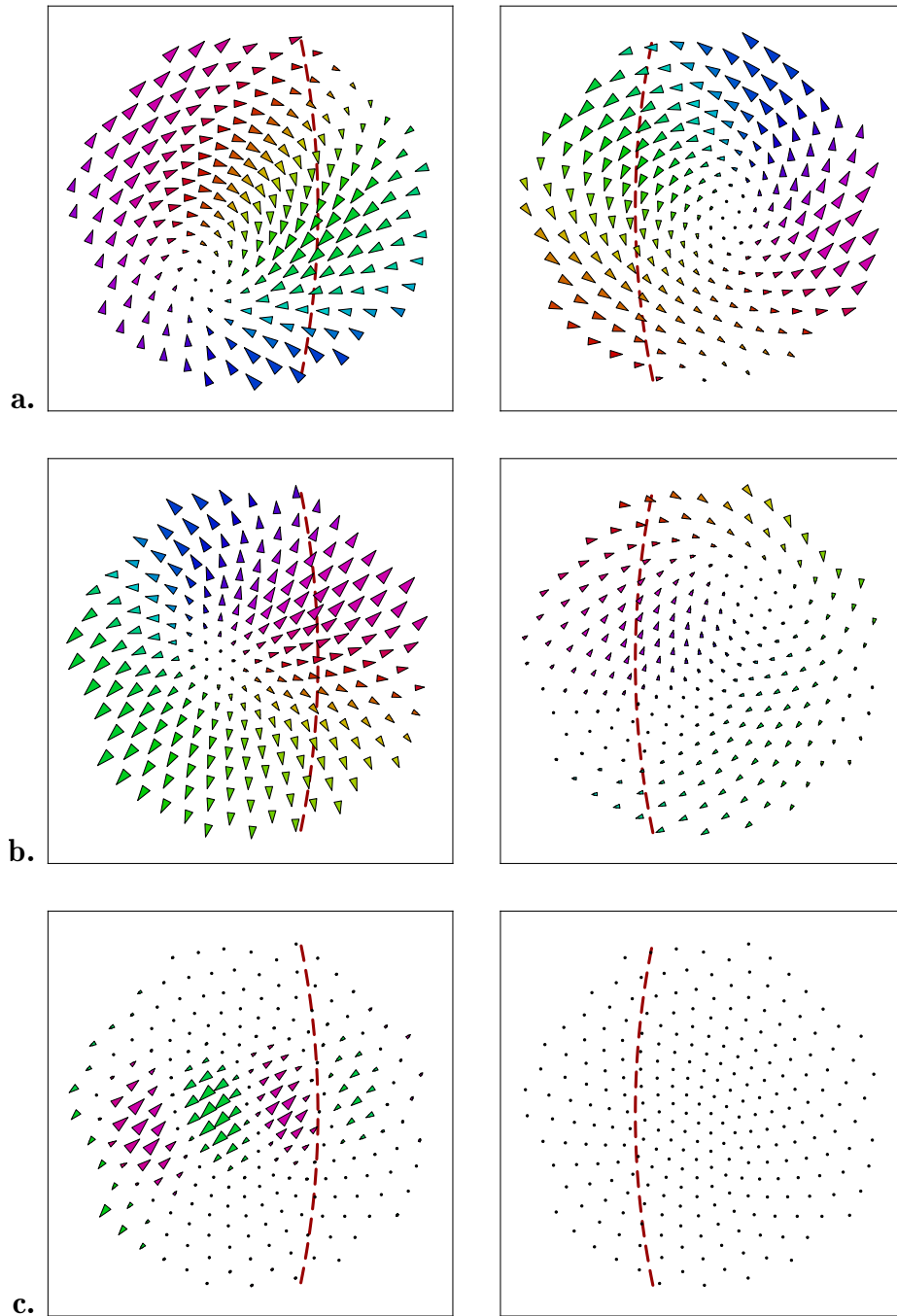


Fig. 2. Sample binocular receptive fields from the sparse coding network. The red dotted lines mark the margin of binocular overlap. **a.** Binocular whole-field neuron with spiral/rotatory characteristic. **b.** Left-dominant whole-field neuron with elliptical focus of expansion in the left eye and a superposition of two curls in the right eye. **c.** Monocular Gabor-field

sequence was recorded from the later (slower) parts of this relaxation. Optic flow was calculated with the FlowNet algorithm [5].

The fish retina was modeled as a spherical shell covering 160 degrees in which 256 sampling points were placed using a simple repulsion algorithm (Fig 1c). The planar camera images were warped by stereographic projection and sampled at these points. For each retinal sampling point i the corresponding local motion vector (u_i, v_i) was represented by two signed variables modeling the activity of pairs of RGCs tuned to opposite motion directions (right/left, and up/down).

3 LCA sparse coding

For learning, we use the LCA sparse coding algorithm [9, 14] which can be summarized as follows. Let $\mathbf{x} = \{x_n\}_{n=1}^N$ denote the input signal, i.e. the output of ganglion cells that signal local retinal motion. In sparse coding, the goal is to reconstruct \mathbf{x} as a linear combination $\mathbf{x} \approx \sum_{k=1}^K a_k \boldsymbol{\varphi}_k$ with dictionary elements $\{\boldsymbol{\varphi}_k\}_{k=1}^K$, and activation coefficients $\{a_k\}_{k=1}^K$, for which sparsity is required [9]. The $\boldsymbol{\varphi}_k$ are vector fields from which the input vector field can be reconstructed as a linear combination. According to [10, 14], each $\boldsymbol{\varphi}_k$ can also be considered as the receptive field of the k -th output neuron, if a specific activation function with feedback is assumed. In our application, the dictionary elements model the receptive fields of K APT neurons. The vector $\mathbf{a} = \{a_k\}$ contains the coefficients needed to reconstruct a given input pattern from the receptive fields. In our simulations, we require $a_k \geq 0$ at all times. If we write the $\boldsymbol{\varphi}_k$ as columns of a matrix $\boldsymbol{\Phi}$ we obtain the error function $E(\mathbf{a}, \boldsymbol{\Phi}) = \frac{1}{2} \|\mathbf{x} - \boldsymbol{\Phi}\mathbf{a}\|_2^2 + S(\mathbf{a})$, in which the first term penalizes reconstruction errors and $S(\mathbf{a})$ penalizes non-sparse vectors \mathbf{a} . While the original algorithm [9] is based on the ℓ^1 -norm, i.e. the total activity of \mathbf{a} , the locally competitive algorithm (LCA) seeks to minimize the ℓ^0 -norm, i.e. the number of non-zero a -values or the number of active units [14]. Since $a_k \geq 0$, this amounts to choosing $S(\mathbf{a}) = \sum_{k=1}^K \lambda \mathcal{H}(a_k - \lambda)$ where \mathcal{H} is the Heaviside function.

For the optimization algorithm see [9, 14]. The algorithm was run in Petavision² with $K = 512$ APT-neurons and 77,076 motion fields each sampled at 256 retinal points for each eye ($N = 1024$). Examples of the resulting $\boldsymbol{\varphi}_k$ are displayed as vector fields in Fig. 2.

4 Backpropagation

The *supervised learning* version of the model used the same retinal encoding scheme and input data described above. Motion sequences were labeled for egomotion by seven continuous variables, three for the unit-vector of heading (translation), three for the unit vector of the

² <http://petavision.github.io/> and [15]

axis of rotation, and a non-negative one for rotational speed. Note that translational speed cannot be recovered from optic flow, so we did not attempt to teach this to the network. The network contained three hidden layers with 1000, 600, and 200 units and an output layer with seven units with the above encoding. The network was implemented in TensorFlow³.

The network was able to recover the heading direction with a mean angular error of about 15 degree and the axis of rotation with a mean angular error of about 19 degree.

5 Results

The simulations produce two types of data, i.e. models of vectorial receptive fields, and neuronal responses to optic flow stimuli. Receptive fields will be discussed only for the sparse coding network since no obvious interpretation was found for the backpropagation case.

Figure 2 shows three typical examples out of the set of 512 φ_k fields. Individual vector fields are generally not realizable as optic flow fields in a rigid environment. For example, Fig. 2a approximates a pitch rotation (nose down) in both eyes, but the axes in the two eyes are not properly aligned. Flow vectors are not purely tangential to the pole but involve a spiral component. Fig 2b shows a left-dominant field with an expansion pattern in the left eye. The focus is elongated as might be expected if two nearby foci would superimpose. The right eye field is a superposition of two rotational poles. We conjecture that “dipole” fields of this type are needed to represent multiple axes of heading and rotation as linear combinations of vector fields. The two receptive fields of Fig. 2a,b have high average a_k values (rank 4 and 10 of the entire set). Fig 2c shows a field with low contribution to the reconstruction (a_k rank 130) which is representative of a large number of fields. It is monocular with clearly delineated lobes of motion preferences in opposite directions, resembling Gabor functions for the horizontal and vertical motion components. Comparable fields have been found with a PCA analysis by [17].

Binocular receptive fields obtained from either learning scheme were further analyzed by calculating their response to spherical rotating or translating grating stimuli as had been used for receptive field mapping in the zebrafish study by [7]. Gratings can move either forward or backward and can be presented to the left, right, or both eyes. Altogether, four monocular and four binocular stimulation types can be distinguished, see Figure 3. Each neuron or model neuron was classified for its reaction to each of the eight stimulus types, resulting in $2^8 = 256$ response types. Of these, 27 optic-flow-related cases are shown in Figure 3 both for the zebrafish recordings (upper histogram) and for the two network simulations (lower histograms). There is also a substantial number of cells not classified for one of the response types.

³ <http://tensorflow.org>

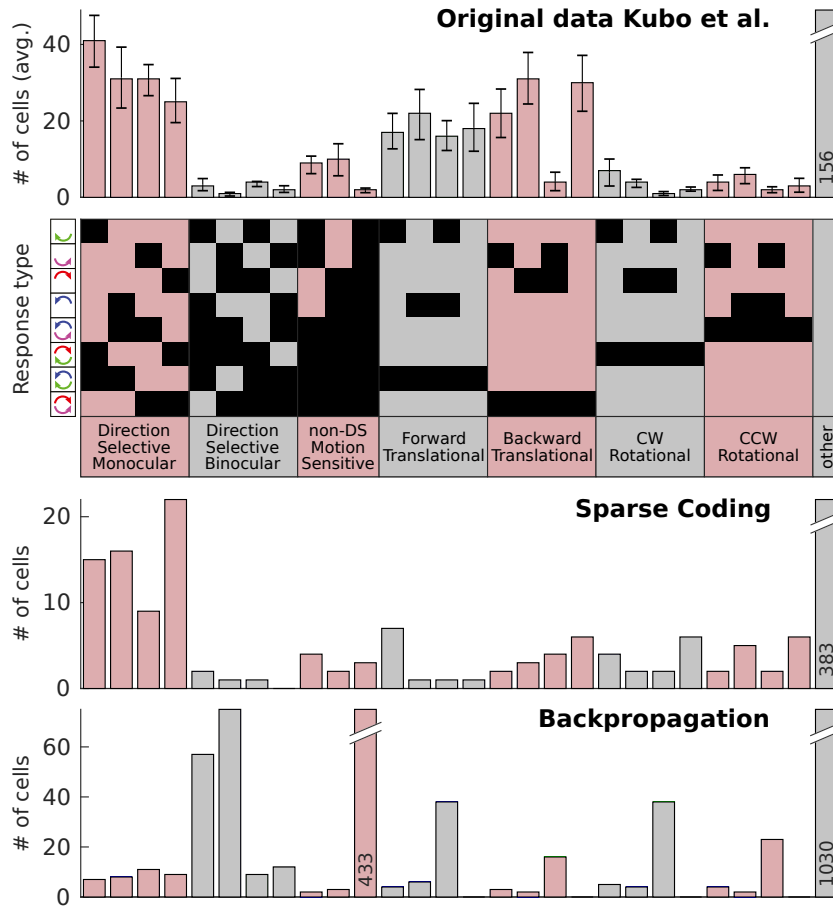


Fig. 3. a. Summary of neuron response characteristics. The top two panels are redrawn from [7]. On the left of the “**Response type**” panel, the little arrows symbolize optic flow stimulation when the fish is heading towards the left, i.e. the first row shows forward optic flow stimulation to the left eye, the second row backwards stimulation to the left eye and so on. The response types are indicated by the columns of black squares. E.g. the first column refers to neurons responding whenever there is forward stimulation to the left eye, irrespective of the stimulus delivered to the other eye, and so on. The histogram on top (“**Original data**”) shows the frequency per fish of neurons of a given response type found in a sample of 3015 cells from six zebrafish larva APT. Most neurons are monocular direction selective (first block). Also, a substantial fraction of neurons specifically responding to global optic flow fields (forward translation etc.) was found. The third panel (“**Sparse Coding**”) shows the results of the present study which are in good general agreement with the fish data. The “**Backpropagation**” block shows the responses of the 1,800 units from all three hidden layers of the supervised learning network, which had been trained to classify optic flow patterns for egomotion.

The response-type group “direction selective monocular” is most frequent in the fish as well as in the sparse coding network, but not in the backpropagation network. It includes neurons that react to the stimulation of one eye, but ignore the stimulus of the other eye. On their own, such neurons cannot analyze egomotion because they cannot distinguish between forward translation and rotation to the contralateral side. However, in the reconstruction approach of sparse coding, they do seem to play an important role in describing the binocular motion fields as well.

The next most frequent response type groups comprise binocular neurons reacting to forward and backward translation, i.e. to patterns that have to be inferred from the stimulus directions in the two eyes. Again, the sparse coding network seems to fit the data better than the backpropagation network.

6 Discussion

In conclusion, receptive fields of zebrafish APT neurons are clearly related to the statistics of environmental stimuli. The sparse coding network seems to be closer to the data, but does not include a mechanism of egomotion recovery. This recovery is implicit in the backpropagation network, but the behavioral relevance of these patterns is not guaranteed. In any case, more work is needed to identify the detailed objective functions reflecting the information requirements of the behaving fish.

Inspection of the vectorial receptive fields learned in the sparse coding network (Fig. 2) suggests that multiple heading directions and axes of rotation are represented by base fields that are not realizable as optic flow templates but provide a basis for linear combination. This is in contrast to the coding by large field templates in the fly [6] and the piecewise construction of optic flow fields from local templates suggested for mammals [13].

References

1. Antinucci, P., Suleyman, O., Monfries, C., Hindges, R. *Current Biology* 26, 1802 – 1815 (2016)
2. Bak-Coleman, J., Smith, D., Coombs, S. *Animal Behaviour* 107, 7 – 17 (2015)
3. Barlow, H.B. *Perception* 1, 371 – 394 (1972)
4. Chalk, M., Marre, O., Tkačik, G. *Proc. Natl. Acad. Sci.* 115, 186 – 191 (2018)
5. Dosovitskiy, A., Fischer, P., Ilg, E., Hausser, P., Hazirbas, C., Golkov, V., van der Smagt, P., Cremers, D., Brox, T.: Flownet: Learning optical flow with convolutional networks. In: *Proc. IEEE Intl. Conf. on Computer Vision*. pp. 2758–2766 (2015)
6. Franz, M.O., Chahl, J.S., Krapp, H.G. *Neural Computation* 16, 2245 – 2260 (2004)
7. Kubo, F., Hablitzel, B., Dal Maschio, M., Driever, W., Baier, H., Arrenberg, A.B. *Neuron* 81, 1344 – 1359 (2014)

8. Nikolaou, N., Lowe, A.S., Walker A.S., Abbas, F., Hunter, P.R., Thompson, I.D., Meyer, M.P. *Neuron* 76, 317 – 324 (2012)
9. Olshausen, B.A., Field, D.J. *Nature* 381, 607 – 609 (1996)
10. Olshausen, B.A., Field, D.J. *Vision Research* 37, 2211 – 3325 (1997)
11. Olshausen, B.A., Field, D.J. *Neural Computation* 17, 1665 – 1699 (2005)
12. Orban, G.A. *Physiological Review* 88, 59 – 89 (2008)
13. Perrone, J.A.: *J. Opt. Soc. Am. A* 9, 177 – 194 (1992)
14. Rozell, C.J., Johnson, D.H., Baraniuk, R.G., Olshausen, B.A. *Neural Computation* 20, 2526 – 2563 (2008)
15. Schultz, P.F., Paiton, D.M., Lu, W., Kenyon, G.T.: Replicating kernels with a short stride allows sparse reconstructions with fewer independent kernels. arXiv preprint arXiv:1406.4205 (2014)
16. Spence, R., Gerlach, G., Lawrence, C., Smith, C. *Biological Reviews* 83(1), 13–34 (2008)
17. Wulff, J., Black, M.J.: Efficient sparse-to-dense optical flow estimation using a learned basis and layers. In: *Proc. IEEE Conf. CVPR*. pp. 120–130 (2015)